Materials and Design 160 (2018) 468–474

Contents lists available at ScienceDirect

Materials and Design

journal homepage: www.elsevier.com/locate/matdes

3D printing of asphalt and its effect on mechanical properties

Richard J. Jackson[a,b], Adam Wojcik[a], Mark Miodownik[a,b,*]

[a]Mechanical Engineering Dept., UCL, London, UK
[b]Institute of Making, UCL, London, UK

HIGHLIGHTS

- We have created a technique to 3D print asphalt — we believe it is the first of its kind.
- 3D printed asphalt is more ductile than cast asphalt.
- The changes in mechanical properties are related to the microstructural changes in asphalt that occur during 3D printing.
- The mechanical properties of 3D printed asphalt depend on process conditions, this can be advantageous allowing toughness to be tailored to the repair.
- The technique has the potential to be used on autonomous vehicles or drones to autonomously repair roads and complex infrastructure.

GRAPHICAL ABSTRACT

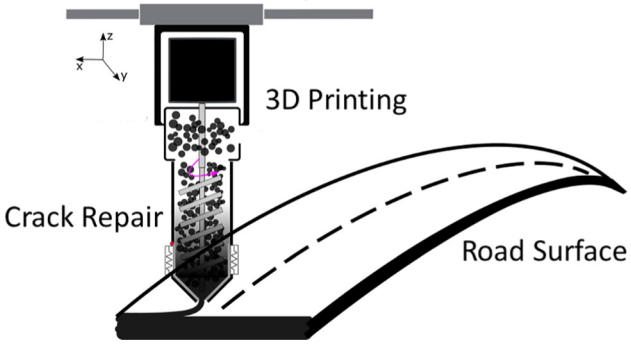

ARTICLE INFO

Article history:
Received 3 May 2018
Received in revised form 13 September 2018
Accepted 14 September 2018
Available online 20 September 2018

Keywords:
Asphalt
Bitumen
3D printing
Additive manufacture
Repair
Toughness

ABSTRACT

The paper describes work to design, build and test an asphalt 3D printer. The main difficulty encountered is that asphalt behaves as a non-Newtonian liquid when moving through the extruder. Thus, the rheology and pressure in relation to set temperature and other operational parameters showed highly non-linear behaviour and made control of the extrusion process difficult. This difficulty was overcome through an innovative extruder design enabling 3D printing of asphalt at a variety of temperatures and process conditions. We demonstrate the ability to extrude asphalt into complex geometries, and to repair cracks. The mechanical properties of 3D printed asphalt are compared with cast asphalt over a range of process conditions. The 3D printed asphalt has different properties from cast, being significantly more ductile under a defined range of process conditions. In particular, the enhanced mechanical properties are a function of process temperature and we believe this is due to microstructural changes in the asphalt resulting in crack-bridging fibres that increase toughness. The advantages and opportunities of using 3D printed asphalt to repair cracks and potholes in roads are discussed.

1. Introduction

Asphalt (bitumen) composites are the most common material used to surface roads, with 95% of UK roads paved with asphalt mixtures [1]. Its success is due to a combination of factors that have been widely studied: it creates a safe and robust road surface for driving when combined with stone aggregates and appropriate polymer binders [2,3]; road surfacing can be carried out rapidly and without complex machinery; it has good acoustic properties and so muffles the sounds of traffic [4]; it is robust, repairable and indeed self-repairs [5-7]. However asphalt composites do degrade

* Corresponding author.
E-mail address: M.miodownik@ucl.ac.uk.

https://doi.org/10.1016/j.matdes.2018.09.030

over time due to the effects of road usage, oxidation, loss of volatiles, moisture damage, and various other factors. This degradation leads to increased stiffness of the road surface, cracks forming, stripping, ravelling, loss of aggregate, and development of pot-holes [8,9].

Despite a stipulated minimum lifetime of 40 years, the re-surfacing of roads is estimated to cost £2 billion per year in the UK alone [10]. Increasing the life of roads has the potential to reduce environmental and financial costs associated with road closures and the congestion they cause. One approach taken to increase the life of asphalt roads has been to enhance their self-healing properties. For instance, mixing ferrous fibres into the asphalt composite allows the material to be heated by induction by the application of an alternating magnetic field [11]. The heating of the fibres locally heats the asphalt and this has been shown in the laboratory to heal micro-cracks and restore the strength of the road, as well as de-icing it [12]. There is currently an on-going trial being carried out in the Netherlands in which a road section has been surfaced with such a material and receives the heating through regular applications of a magnetic field via a specially adapted vehicle [13]. Other approaches to preventing road surface degradation are the inclusion of micro-capsules of sunflower oil into the asphalt composite which burst open in the presence of a crack and increase the fluidity of the asphalt allowing it to reflow and heal the crack [14].

Environmental considerations have led to much interest in the use of recycled materials such as rubber and plastic in asphalt composites [15,16]. These materials are often inexpensive, being currently considered as waste, but the asphalt mixing phase is energy intensive [17,18] and the cost of transport is also a factor [19]. So when looking to increase the environmental sustainability of infrastructure maintenance, materials and repair processes should ideally be optimised together. In the future, many of these demands could be met by autonomous vehicles which repair locally on demand [20]. In the case of asphalt roads, this optimised preventative approach to road maintenance would need to focus on the early stages of road degradation when small cracks form on the road surface. These cracks allow water ingress and grow rapidly during freeze-thaw cycles through the de-bonding of aggregates to form potholes. Once formed it is very hard to stop the growth of these potholes which cause significant vehicle damage and so lead to shortening of the usable lifetime of the road.

This paper describes work to produce a 3D printing technology that could be attached to an autonomous vehicle or drone, and used to repair small cracks before they turn into potholes. 3D printing is a method by which objects can be fabricated layer by layer from a CAD model of the object. By scanning a road surface the negative shape of the crack can be obtained and processed into a 3D model [21]. This information can then be processed and passed to a 3D printer, which can then print exactly the correct amount of material to conform to the crack shape and volume, thus repairing the crack. 3D printing technology has previously been used to repair spall damage in concrete road surfaces [22]. We show for the first time that it is also possible to 3D print asphalt into a crack to restore the road surface. The focus of this paper is a description of the design and operation of our asphalt 3D printer, a demonstration of its ability to repair cracks, and an investigation of the mechanical properties of the 3D printed asphalt.

2. Materials & methods

The 3D printer is designed as a three axis system in which the extrusion nozzle is moved by individual stepper motors to print onto a flat bed, see Fig. 1 (a). The printer nozzle consists of an auger screw, a stepper motor to drive the screw, and a pellet hopper to take asphalt in the form of pellets. The pellets are softened as they travel through the auger screw by an increase in temperature due to the action of heating resistors, this results in a fluid flow of asphalt out of the nozzle, as illustrated in Fig. 1 (b). The stepper motors, temperature, temperature gradient, and auger screw rotation rate are controlled by simple electronics interfaced to a PC, shown schematically in Fig. 1 (c).

The 3D printer was constructed using an existing frame and control system from a RepRap Mendel 90 3D printer, see Fig. 2 (a). The extrusion nozzle assembly was 3D printed using a Form 2 Stereolithography 3D printer using the Formlabs proprietary high temperature acrylic based resin which allowed precise control of the complex geometry of the extruder housing and auger screw (attached to the stepper motor shaft via 5 mm grub screw), see Fig. 2 (b). The extruder assembly had an inner heating sleeve made from a 1 mm thick, 20 mm outer diameter aluminium pipe, with the 15 W 20 Ω Caddock MP915 series TO-126 power resistors attached radially, spaced 120° apart, and connected in parallel. These were attached to the outer part of the pipe with MG Chemicals two-part silver epoxy/cold solder. The temperature was measured using a 100 k EPCOS B57550G1104F thermistor. The thermistor was attached to the aluminium pipe by drilling a 0.5 mm deep indentation into the pipe with a 2 mm drill bit approximately 5 mm away from one of the power resistor contact points, and similarly fixed with silver epoxy. Heat conduction through the aluminium pipe to the extrusion tip proved to be insufficient to control the asphalt temperature quickly and accurately enough and so a metal nozzle cap was employed to improve heat conduction to the asphalt. This was initially made from CNC machined aluminium but the same results were obtained by concentrically stacking M8, M4 and M2 stainless steel washers at the nozzle tip and fixing to each other and the pipe with silver epoxy, see Fig. 2 (b). Conventional fused deposition modeling (FDM) via another, unmodified Mendel 90 RepRap printer was used to print the stepper motor housing and PCB and serial port clip in ABS plastic. Fig. 2 (c) shows a photo of the extrusion nozzle.

By selecting the hardest grade of bitumen, 10/20, we hoped to match the in-use material properties as much as possible [1]. The asphalt pellets were formed from larger pieces of asphalt (Bitumen, CAS 64742-93-4, 10/20 grade, material and data sheet supplied by IKO PLC, UK [23]) by low temperature casting (below 150 °C) into a machined mould to obtain millimeter scale pellets. Asphalt is a substance made principally of long-chain hydrocarbon molecules in a colloidal structure of aphaltenes and maltenes with complex rheological properties [24]. Above a threshold temperature, typically between the range of 30–70 °C, it behaves as a Newtonian fluid. Below this threshold, it undergoes shear-thinning. The rheology in this regime has been studied in detail and shows an Arrhenius-like behaviour [25]. Much work has been done to study the effect on rheology of polymeric binders that are added to asphalt, these behave as viscoelastic components [26]. In the face of this complexity, we chose not to try to model the regime of rheology under different shear stresses as the asphalt pellets travelled through our extruder, but instead we aimed to find the optimum processing variables by carrying out a systematic empirical investigation of the extrusion process.

We identified the important design parameters of the nozzle through a number of design iterations, see Fig. 3 (a). Using infrared cameras to identify thermal gradients allowed us to understand the heat flow within the extruder and so iterate the design towards optimum parameters. The power limit ($P = 45$ W) and torque limit ($T = 44$ N cm) of the three power resistors and stepper motor respectively, were self-imposed design constraints. A number of auger screw designs were fabricated and systematically tested within the printer framework. Chamber height, in combination with screw height and metal insert height was found to be important as an interim asphalt softening area was needed in between the hopper and screw, otherwise the screw would stall, or break, trying to extrude asphalt which was too viscous. For this reason, the final design has zero unheated chamber height. We found that for temperatures above 150 ° C, the asphalt was so fluid it flowed out of

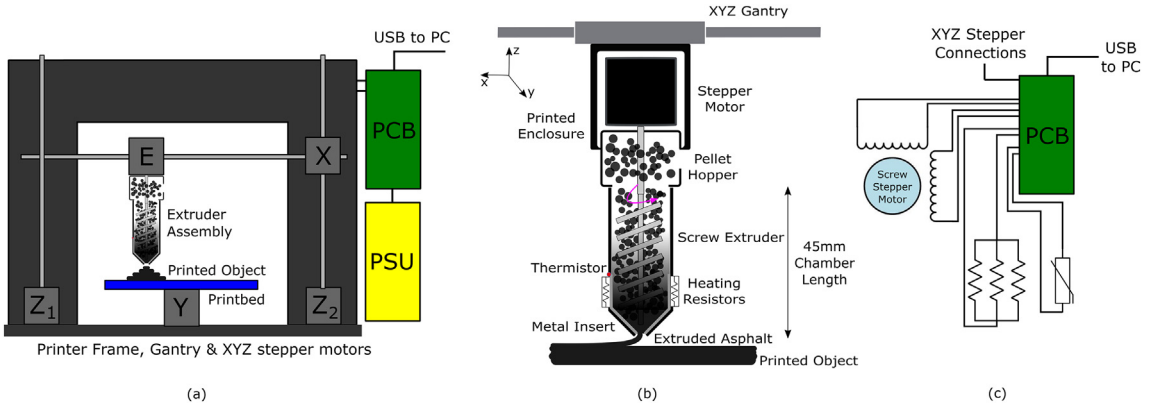

Fig. 1. System design: (a) 3D printer, (b) the extruder design, (c) the control electronics.

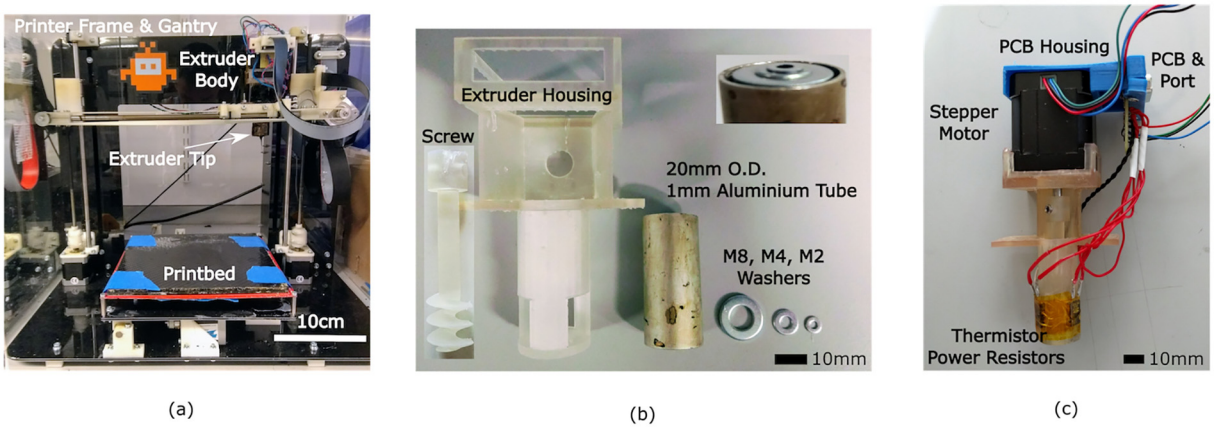

Fig. 2. Experimental: (a) photo of whole system, (b) photo of extruder components, (c) photo of complete extruder.

the extruder aperture under no screw rotation so was not useful for 3D printing.

The temperature range of 100–140° C was explored to print a range of test objects. Screw length and pitch affect the extrusion rate for a given rotations per minute (RPM) but this was not investigated. Various extrusion diameters from 0.5 to 5 mm were used with 2.5 mm found to give the best balance between reliability and dimensional accuracy. Print failures were identified by incomplete or poor first layer adhesion, intermittent layer bonding, incomplete printing, and partially hollow objects. Our final design of the extrusion nozzle is shown in Fig. 3 (b) with the following parameters: the chamber diameter ($d_c = 17.5$ mm), metal insert height ($h_i = 47.5$ mm), the tip height ($h_t = 2.5$ mm), the unheated chamber height ($h_u = 0$ mm), the extrusion diameter ($d_e = 2.5$ mm), the auger screw length ($l_s = 21$ mm), pitch ($p_s = 7$ mm) and the total thermal input area ($A_t = 270$ mm^2).

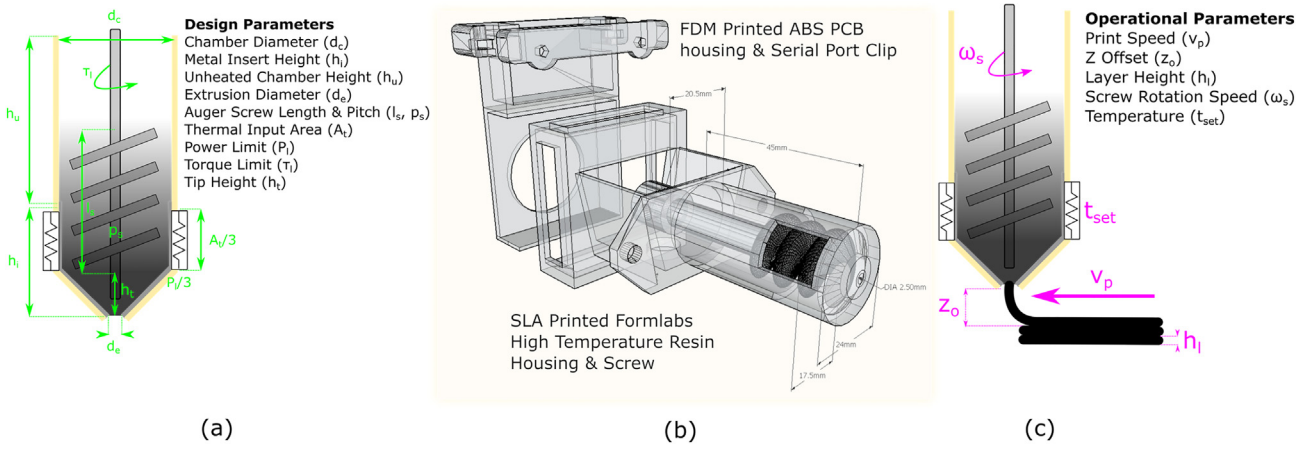

Fig. 3. Design parameters: (a) CAD of extruder, (b) design parameters, (c) process parameters.

Using this design, we found that the optimum operational parameters of the extrusion nozzle were the print speed ($v_p = 1$ mm/s), the z offset ($Z_o = 3$ mm), the layer height ($l_h = 3$ mm), the auger screw rotation speed ($W_s = 5$–10 RPM), the set temperature ($t_{set} = 125$–135 ° C), see Fig. 3 (c).

We used open access Pronterface control software (version 3) [27] and Slic3r slicing software [28] to generate g-code and print via standard STL files designed using the 3D CAD software Sketchup [29]. The Slic3r software is intended for use with fused deposition modelling (FDM) printers which heat a filament of defined diameter through the heated extruder hole. As such, the filament diameter setting was used as the extruder chamber diameter to represent the width of the asphalt, however this is not completely accurate as the auger screw takes up a significant proportion of the chamber volume. Furthermore, the Slic3r "extrusion multiplier" setting is intended to increase or decrease the filament feed speed to the extruder, whereas in our case the filament feed motor was used as the auger screw motor (100× extruder multiplier was found to be equivalent to 4.4 RPM). An optimisation process was used to set these heat and print speed settings.

A number of different shapes were printed including standard mechanical test bars with dimensions 80 × 10 × 6 mm. These were mechanically tested at room temperature measured as 22 °C using a three point bend test rig on a Hounsfield HK5 universal testing machine one week after printing or moulding. The tests were carried out with a 2500 N load cell at constant strain rate of 1 mm/min with support bars spaced 25 mm apart. For each test condition, six samples were tested and the data aggregated. A number of cast asphalt samples were also produced to compare with the 3D printed samples. These were cast into PDMS moulds with the same dimensions as the mechanical test bars at 150 °C. The time between casting, 3D printing and mechanical testing was 48 h.

3. Results

Firstly, basic 3D printing experiments were carried out in which three single lines of asphalt of length 100 mm were printed with 1 mm layer height using an aperture width of 2 mm. These experiments were performed using a range of print-head temperatures between 100 and 150 °C. Temperatures between 125 °C and 135 °C were found to be optimal to create a continuous extrusion of asphalt with a consistent line width. The rotation speed of the auger screw, W_s, was found to be an important variable that determined the line thickness. Fig. 4 shows the effect of W_s on the line thickness of the 3D printed asphalt at 125 °C. Line printing was less successful and reliable at lower rotation speeds (approximately 2–7 RPM) although this was not an issue when printing objects, as subsequent layer deposition and adhesion after the first layer was helped by (and was reliant on) the initial layer. Nonetheless above 5 RPM we were able to reliably print single lines.

Fig. 5 (a) shows the ability of the 3D printer to fabricate an object from a digital CAD file through the layering of lines of asphalt, in this case the shape is a pyramid, but this technique is general, with the same object geometry limitations as standard polymer prints. The print layers are clearly visible and approximately 1 mm in height. Some flow and bleeding of the asphalt is visible which affects the feature resolution of the object. Fig. 5 (b) shows the ability of the system to 3D print a mechanical test sample of known proportions for mechanical testing. A number of such samples were printed in which a number of geometry and process variables were varied. The temperature range of 125–135°C at 1 mm/s print speed and 4.4 RPM (100× extrusion multiplier) gave the most accurate and reliable prints in terms of desired dimensions and the success of printing a fully formed object. These test samples were then mechanically tested using a 3 point bend test together with cast asphalt test sample of identical dimensions. Fig. 5 (c) shows the ability of the system to take as an input the inverted shape of a crack in an asphalt sample and 3D print asphalt into the crack to fill it.

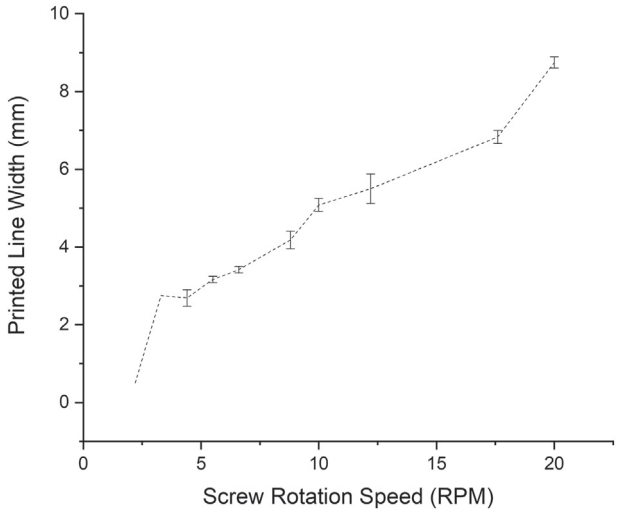

Fig. 4. Results: Graph of effect of screw rotation speed on printed line thickness.

Fig. 6 shows the stress/strain curves obtained from cast asphalt and compares them to those from 3D printed asphalt at three different printing temperatures. It can be seen that the mechanical properties are markedly different for the two fabrication methods. For the cast samples there was, as expected, anisotropy observed between those samples tested with their bottom or top surfaces under compression, see Fig. 6 (a). The former showed a classic brittle fracture while the latter showed some ductile behaviour before fracture, see Fig. 6 (d). This anisotropy is likely due to the differences in their surface roughnesses, porosity, and volatile content between the top and bottom of the sample. There were no differences seen in testing the 3D printed samples from top or bottom. Both sets of samples showed similar fracture strengths, see Fig. 6 (c). The 3D printed specimens showed up to nine times the ductility of cast samples but had similar fracture strengths of around 2 MPa, see Fig. 6 (b). The toughness of the moulded and 130 ° C printed samples were found to be 10.2 ± 7.1 and 24.1 ± 7.2 J/cm^2 respectively.

The effect of extrusion temperature on mechanical properties is small although there is some evidence that 130 °C is optimal, see Fig. 6 (a). Observation of the fracture surfaces provides some explanation for the difference in ductility between the cast asphalt and the 3D printed asphalt. When the printed samples were cracked, a brown substance was revealed which was dotted throughout the sample cross section, that in many cases stretched out to bridge the crack, see Fig. 7. This brown phase and crack bridging effect were not observed in the cast test samples. Using X-ray photoelectron spectroscopy (XPS), the elemental composition of the brown phase was compared to the bulk. No significant differences were found in the composition, both being hydrocarbons with trace amounts of silicon and sulphur.

4. Discussion & implications for design

We have successfully managed to design, build and test an asphalt 3D printer capable of printing small objects and repairing cracks in asphalt. Since 3D printers are a mature technology this might not seem remarkable, nevertheless it was not an easy task. The main difficulty we encountered is that asphalt behaves as a relatively low melting point non-Newtonian liquid when the material is moving through the extruder as it is heated up, and then in

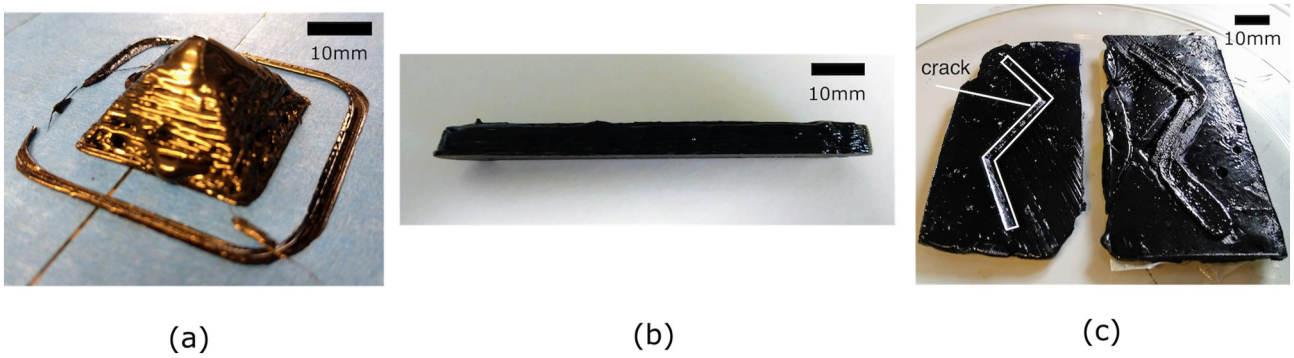

Fig. 5. Results: (a) photo of printed pyramid, (b) photo of three point bend test sample, (c) photo of moulded crack before (left) and after print fill (right).

between the extruder tip and deposition surface, as it cools down. Although polymers used in filament-fed 3D printers are generally non-Newtonian too, their simpler extruder system makes flow control much easier. Flow through our auger screw extruder created a more complicated regime of rheology and pressure in relation to set temperature and other operational parameters which showed highly non-linear behaviour and made control of the extrusion process difficult. The functional constraints of some of the process variables affected our ability to print, for instance, the rotation speed of the auger screw is linked to the print speed (the extrusion multiplier is programmed to double the rotation speed if the print speed is doubled in order to deposit material at the same rate). The print speed was also limited by the materials properties of the auger screw (we used the high temperature SLA resin), since the low fracture strength of this resin limited the torque we could apply. The aperture affects the resolution of the printer, but again, low fracture strength of SLA resin limited our ability to reduce aperture size since it led to high pressures and resulted in mechanical failure. It is hoped that

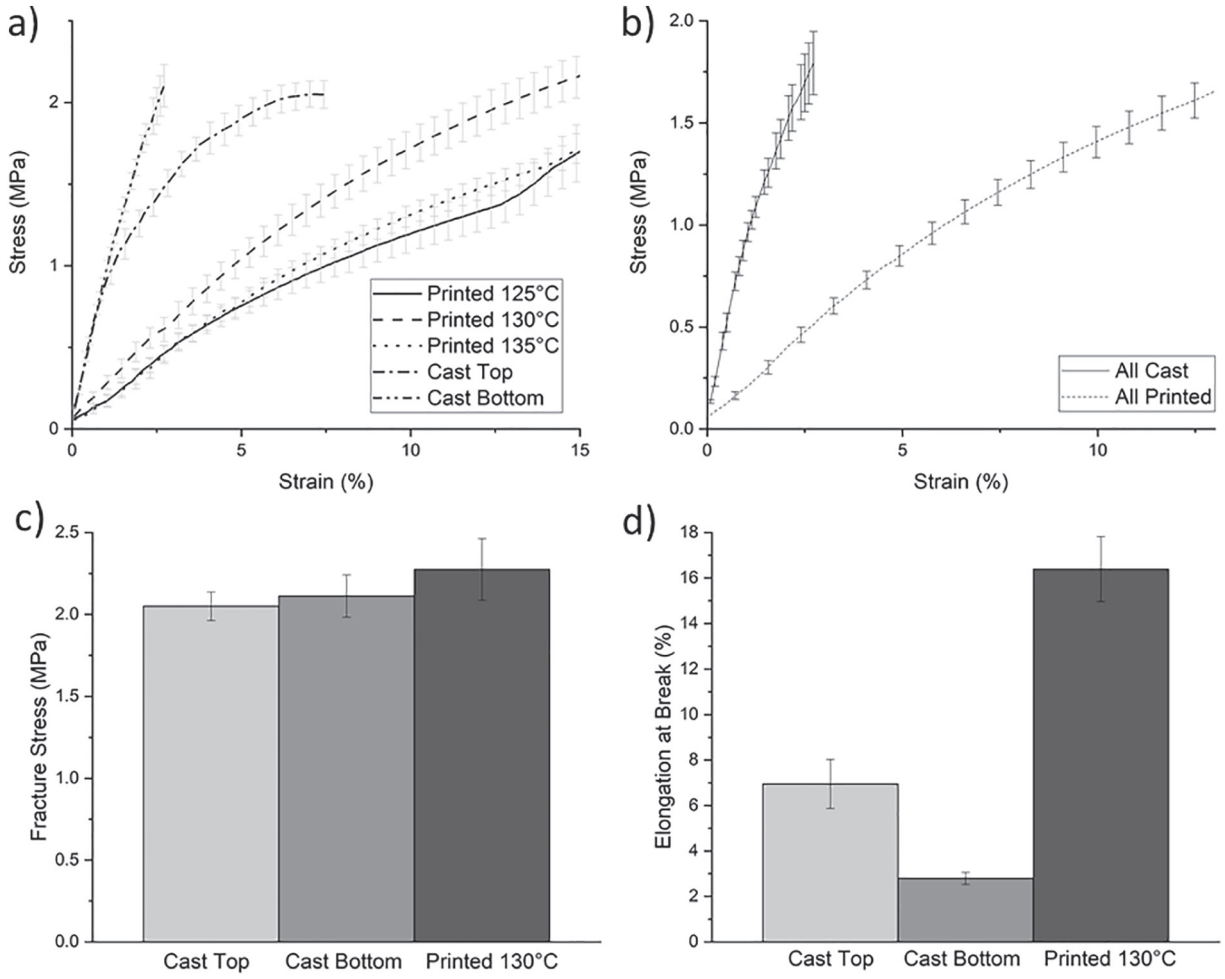

Fig. 6. Mechanical properties: 3 point bend tests. (a) Cast pieces average, tested from top (CT) and bottom (CB) compared to print averages at each temperature. (b) Comparison of all cast and printed pieces. (c) Stress at fracture comparison. (d) Elongation at break comparison.

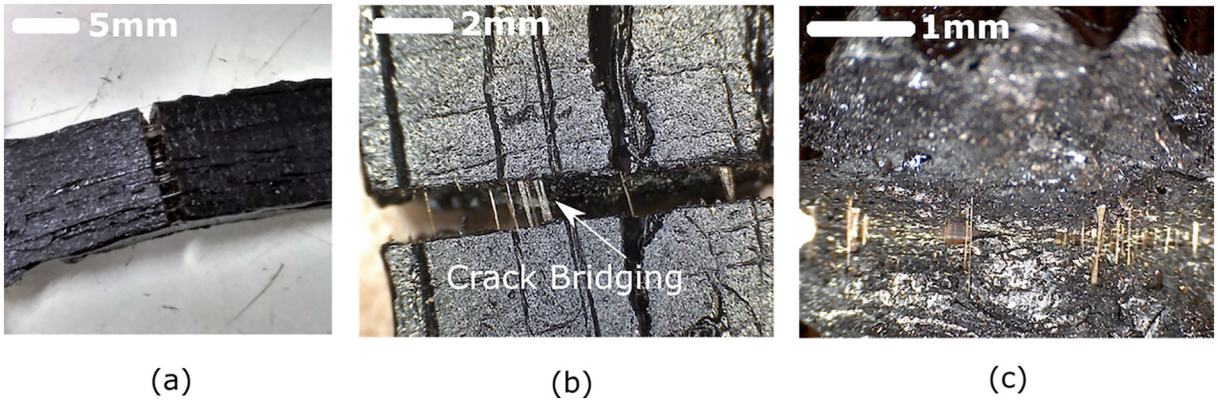

Fig. 7. Crack bridging: (a) bridging in printed test samples, (b) closeup, parallel to sample axis shows fibrous crack bridging characteristic of ductile fracture, (c) 20× magnification showing concentration of oily material throughout print layers. (For interpretation of the references to color in this figure, the reader is referred to the web version of this article.)

future designs with metal parts will allow us to explore a greater range of extrusion rates and print resolutions.

The impact of 3D printing on mechanical properties is interesting because it allows us to print a more ductile asphalt. There is a significant increase (up to 900%) in elongation to fracture for the printed samples. A possible explanation of this increased ductility lies with the appearance of a crack bridging component in the samples. It is hypothesised that the brown phase precipitated throughout the sample is composed of a lighter saturated fraction of the asphalt that has coalesced due to size dependent mobility conditions during the heating, screw mixing and/or extrusion process. Small amounts of softer components coalesce naturally in asphalt, but usually at scales of around 1–10 μm [30]. Here, the components are around 20–100 μm in diameter. This means that the 3D printing process at this scale seems to avoid the degradation of its mechanical properties that can arise from leaving molten asphalt static for a long time [31]. The 3D printing process seems to create a composite structure comprising of large concentrations of the brown phase dotted throughout the asphalt (as seen in Fig. 7 (c)), giving the material a higher toughness than cast asphalt. This would be advantageous to any crack repair scenario since sites of cracks on roads are often areas of increased stress or wear, and so depositing material with enhanced ductility could prolong the life of the repair.

Printed asphalt extruded at less than 120 ° C often did not have sufficient inter-layer bonding to avoid delamination, so were most likely not fully bonded throughout the bulk of the material. Conversely, prints above 135 ° C gave poor dimensional accuracy due to the lower viscosity of the hotter deposited asphalt, as well as showing mechanical properties similar to cast samples. This suggests that there is a point between delamination and complete intermelting that gives superior mechanical properties, we found this to be the optimum print temperature of 130 ° C. Commonly printed polymers such as ABS and PLA have lower specific heat capacities than asphalt (1.8, 1.3, and 2.1 kJ/kg/° C respectively) which may be the reason why the initial printing temperature may occasionally be too high as the print progresses due to heat build up in the printed asphalt, giving melted edges and/or poor accuracy, and particularly a “squashed” appearance with too low object height and too high object width and length. Over the print time (approximately 20 min for the test bar) this would be enough to deform layers previously printed due to the excess heat in the upper layers. Although the printer bed is heated for conventional polymer printing we did not employ this method nor did we use a cooling fan normally used with polymer 3D Printing, which may have exacerbated the issue. With the correct parameters however, we can modulate properties through changing print temperature fairly rapidly over a small 10–15 ° C range. Furthermore, the feed and pellet system make it relatively straightforward to add other materials such as small microaggregates or nanomaterials (initial test prints with 10% 10 nm diameter titanium dioxide nanoparticles have been successful), and then vary the composition of the feedstock during printing to create more complex, functionally graded infrastructure materials with a wider range of properties.

We believe these improved and tunable material properties of 3D printed asphalt, combined with the flexibility and efficiency of the printing platform, offers a compelling new approach not just to the maintenance of road infrastructure, but by attaching it to a drone, opens up a new way to repair hard to access structures such as the flat roofs of buildings and other complex structures. The advantage of this is not only in being able to cut costs – other repair methods often requiring the erection of scaffolding and the closure or shutting down of infrastructure to gain access – but also the repair can initiated earlier before large scale deterioration has occurred. The development of such repair drones would have implications both for the way in which city infrastructure is repaired but also for the economic model that underpins it. At the moment, much of city infrastructure is built to fail and then be replaced, with the capital costs of construction dominating the design parameters. Infrastructure designed to be continually monitored and repaired by fleet of drones promises to be a different model which could have economic benefits to society.

For instance, such an approach has the potential to be used for roads. If road degradation is continually monitored then small cracks can be repaired before they turn into potholes. By intervening at this early stage and repairing the crack autonomously using 3D printing we believe the road surface might be preserved for longer. Such approaches have been explored for concrete road surfaces for spall damage repair [22]. We have already demonstrated the 3D printing of asphalt using a drone. The next stage of developing this technology involves understanding the effect of environmental variables such as road temperature, air temperature, the local chemistry, interface with aggregate, as well as more comprehensive testing such as cyclic loading of repaired crack roads.

The materials science of repair is not the only consideration in the application of this technology. Identification and detection of crack morphology, especially in the case of complex-shaped cracks will be an important challenge. Automated computer vision systems are currently being explored to address this issue [20]. The use of gantry systems versus the employment of 6-axis robotic systems is another design issue that is pertinent in the area of automated construction and repair [32,33]. Although 6-axis systems have more flexibility; for the repair of sub-cm small cracks in a horizontal road surface, a simple gantry system, such as ours, may well prove effective enough.

5. Conclusions

We have designed and built 3D printer capable of printing asphalt. We have shown that this technology can be used to 3D print asphalt into complex geometries, and to repair cracks. The mechanical properties of 3D printed asphalt are different from cast asphalt, showing up to nine times the ductility of cast samples with similar fracture strengths. The increased ductility is due to microstructural changes in the asphalt which result in crack-bridging fibres that increase toughness. The material properties of 3D printed asphalt are tunable, and combined with the flexibility and efficiency of the printing platform, this technique offers a compelling new design approach to the maintenance of infrastructure.

Acknowledgments

This work was funded by the EPSRC (Balancing the Impact of City Infrastructure Engineering on Natural systems using Robots — EP/N010523/1). We would like to thank Professor Quentin Pankhurst for access to laboratory facilities, and Dr Joseph Bear at Kingston University for the XPS analysis. We would also like to thank all members of Self-Repairing Cities network.

References

[1] IAT, Asphalt Professionals in the 21st Century, 2000.
[2] S. Chi, B.R.K. Blackman, A.J. Kinloch, A.C. Taylor, Durability of asphalt mixtures: effect of aggregate type and adhesion promoters, Int. J. Adhes. Adhes. 54 (2014) 100–111.
[3] The Asphalt Paving Industry: A Global Perspective, 3rd ed. ed., Number ISBN 0-914313-06-1 in Global Series 101, National Asphalt Pavement Association and European Asphalt Pavement Association, Lanham, Maryland, 2011.
[4] U. Sandberg, Low Noise Road Surfaces a State-of-the-art Review, The Mitigation of Traffic Noise in Urban Areas, 1992, volume Eurosymposium, May.
[5] A. Garcia, Self-healing of open cracks in asphalt mastic, Fuel 93 (2012) 264–272.
[6] Y. Tan, L. Shan, Y.R. Kim, B. Underwood, Healing characteristics of asphalt binder, Constr. Build. Mater. 27 (1) (2012) 570–577.
[7] J. Norambuena-Contreras, A. Garcia, Self-healing of asphalt mixture by microwave and induction heating, Mater. Des. 106 (2016) 404–414.
[8] P.K. Das, H. Baaj, N. Kringos, S. Tighe, Coupling of oxidative ageing and moisture damage in asphalt mixtures, Road Mater. Pavement Des. 16 (2015) 265–279.
[9] A.A. Butt, B. Birgisson, N. Kringos, Considering the benefits of asphalt modification using a new technical life cycle assessment framework, J. Civ. Eng. Manag. 22 (5) (2015) 597–607.
[10] UK Dept. of Transport Highways Agency, Design Manual for Roads and Bridges, 2006.
[11] Q. Liu, A. Garcia, E. Schlangen, V. Martin van de, Induction healing of asphalt mastic and porous asphalt concrete, Constr. Build. Mater. 25 (2011) 3746–3752.
[12] H. Fang, Y. Sun, Q. Liu, B. Li, S. Wu, J. Tang, Ice melting properties of steel fiber modified asphalt mixtures with induction heating 2017, IOP Conf. Ser. Mater. Sci. Eng. 182 (1) (2017).
[13] Q. Liu, H. Schlangen, G. Van Bochove, The first engineered self-healing asphalt road: how is it performing? ICSHM 2013: Proceedings of the 4th International Conference on Self-healing Materials, Ghent, Belgium, 16-20 June 2013, 2013.
[14] A. Garcia, C.A. Austin, J. Jelfs, Mechanical properties of asphalt mixture containing sunflower oil capsules, J. Clean. Prod. 118 (2016) 124–132.
[15] Y. Huang, R.N. Bird, O. Heidrich, A review of the use of recycled solid waste materials in asphalt pavements, Conserv. Recycl. Resour. 52 (1) (2007) 58–73.
[16] D.L. Presti, Recycled tyre rubber modified bitumens for road asphalt mixtures: a literature review, Construction and Building Materials 49 (2013) 863–881.
[17] P. Zapata, J. Gambatese, Energy consumption of asphalt and reinforced concrete pavement materials and construction, J. Infrastruct. Syst. 11 (1) (2005).
[18] Y. Huang, R. Bird, O. Heidrich, Development of a life cycle assessment tool for construction and maintenance of asphalt pavements, J. Clean. Prod. 17 (2) (2009) 283–296.
[19] A.A. Butt, I. Mirzadeh, S. Toller, B. Birgisson, Life Cycle Assessment framework for asphalt pavements; methods to calculate and allocate energy of binder and additives, Int. J. Pavement Eng. 15 (4) (2014) 290–302.
[20] R. Fuentes, T. Chapman, M. Cook, J. Scalan, Z. Li, R.C. Richardson, Briefing: UK-RAS white paper in robotics and autonomous systems for resilient infrastructure. Volume 170 Issue SC3 72-79, Smart Infrastruct. Construct. 3 (2017) 72–79.
[21] T. Kim, S. Ryu, Review and analysis of pothole detection methods, J. Emerg. Trends Comput. Inf. Serv. 5 (8) (2014) 603–608.
[22] J. Yeon, J. Kang, W. Yan, Spall damage repair using 3D printing technology, Autom. Constr. 89 (2018) 266–274.
[23] IKO PLC, Easymelt Bonding Bitumen - CAS 64742-93-4, 2018.
[24] L. Loeber, G. Muller, J. Morel, O. Sutton, Bitumen in colloid science: a chemical, structural and rheological approach, Fuel 77 (13) (1998) 1443–1450.
[25] A. Rabbani, D.R. Schmitt, Ultrasonic shear wave reflectometry applied to the determination of the T shear moduli and viscosity of a viscoelastic bitumen, Fuel 232 (2018) 506–518.
[26] E. Remišová, V. Zatkaliková, F. Schlosser, Study of rheological properties of bituminous binders in middle and high temperatures., Civ. Environ. Eng. 12 (2016) 13–20.
[27] Pronterface, 2012, http://www.pronterface.com/.
[28] Slic3r, 2011, http://slic3r.org/.
[29] Sketchup, 2000, https://www.sketchup.com/.
[30] A. Jager, A. Lackner, C. Eisenmenger-Sittner, R. Blab, Identification of microstructural components of bitumen by means of atomic force microscopy, Proc. Appl. Math. Mech. 4 (2004) 400–401.
[31] B. Hofko, A. Falchetto, J. Grenfell, L. Huber, X. Lu, L. Porot, L. Poulikakos, Z. You, Effect of short-term ageing temperature on bitumen properties., Road Mater. Pavement Des. 18 (2017) 108–117.
[32] C. Gosselin, R. Duballet, P. Roux, N. Gaudillière, J. Dirrenberger, P. Morel, Large-scale 3D printing of ultra-high performance concrete—a new processing route for architects and builders, Mater. Des. 100 (2016) 102–109.
[33] Y.W.D. Tay, B. Panda, S.C. Paul, N.A. Noor Mohamed, M.J. Tan, K.F. Leong, 3D printing trends in building and construction industry: a review., Virtual Phys. Prototyping 12 (3) (2017) 261–276.